Our findings provide insights into the atomic-scale fundamental processes of ultra-thin film lubrication, thus extending continuum EHL and micro-EHL treatments into the nanometer realm. Such investigations address some issues facing certain current novel technologies [such as high-density information storage and retrieval systems (*20*) and provide the impetus for future experimental and theoretical investigations.

REFERENCES AND NOTES

1. F. P. Bowden and D. Tabor, *Friction* (Anchor Press–Doubleday, Garden City, NY, 1973); *The Friction and Lubrication of Solids* (Clarendon, Oxford, 1950), part I; *ibid.* (Clarendon, Oxford, 1964), part II.
2. A. Cameron, *Principles of Lubrication* (Longman, London, 1966).
3. D. Dowson and G. R. Higginson, *Elastohydrodynamic Lubrication* (Pergamon, London, 1977).
4. R. Gohar, *Elastohydrodynamics* (Horwood, Chichester, England, 1988).
5. D. Dowson and V. Wright, Eds., *An Introduction to the Bio-Mechanics of Joints and Joint Replacements* (Mechanical Engineering, Edmunds, United Kingdom, 1978); see also (*11*), p. 485.
6. See review by D. Dowson, in *Fundamentals of Friction: Macroscopic and Microscopic Processes*, I. L. Singer and H. M. Pollock, Eds. (Kluwer, Dordrecht, Netherlands, 1992), p. 325.
7. See articles in (*6*); for a recent review, see B. Bhushan, J. N. Israelachvili, U. Landman, *Nature* **374**, 607 (1995).
8. U. Landman, R. N. Barnett, H.-P. Cheng, C. L. Cleveland, W. D. Luedtke, in *Computations for the Nano-Scale*, P. E. Bloch, C. Joachim, A. J. Fisher, Eds. (Kluwer, Dordrecht, Netherlands, 1993), p. 75; P. A. Thompson, M. O. Robbins, G. S. Grest, *ibid.*, p. 127.
9. See J. A. Greenwood in (*6*), p. 37 and p. 57.
10. S. M. Foiles, M. I. Baskes, M. S. Daw, *Phys. Rev. B* **33**, 7983 (1986).
11. J. P. Ryckaert and A. Bellemans, *Discuss. Faraday Soc.* **66**, 95 (1978).
12. T. K. Xia, J. Ouyang, M. W. Ribarsky, U. Landman, *Phys. Rev. Lett.* **69**, 1967 (1992).
13. U. Landman, W. D. Luedtke, J. Ouyang, T. K. Xia, *Jpn. J. Appl. Phys.* **32**, 1444 (1993).
14. M. P. Allen and D. J. Tildesley, *Computer Simulations of Liquids* (Clarendon, Oxford, 1987).
15. S. Granick, *Science* **253**, 1374 (1991).
16. J. Gao, W. D. Luedtke, U. Landman, *Langmuir*, in press.
17. It is of interest to note that a similar value for the yield pressure was obtained by us in previous studies of nanoindentation and elongation of gold [U. Landman, W. D. Luedtke, N. A. Burnham, R. J. Colton, *Science* **248**, 454 (1990); U. Landman and W. D. Luedtke, *J. Vacuum Sci. Technol. B* **9**, 414 (1991)]. This value is an order of magnitude larger than the yield stress of macroscopic gold samples, reflecting the plastic nature of the mechanical deformation in nanometer-scale metal structures.
18. U. Landman and W. D. Luedtke, *Mater. Res. Soc. Bull.* **17 (5)**, 36 (1993).
19. X. Ai, H. S. Cheng, L. Zheng, *ASME J. Tribol.* **115**, 102 (1993); L. Chang, A. Jackson, M. N. Webster, *Tribol. Trans.* **37**, 435 (1994).
20. B. Bhushan, *Tribology and Mechanics of Magnetic Storage Devices* (Springer, New York, 1990).

21. Supported by the U.S. Department of Energy, NSF, and the Air Force Office of Scientific Research. Computations were performed on CRAY Computers at the National Energy Research Supercomputer Center, Livermore, CA, at the Pittsburgh Supercomputing Center, and at the Georgia Institute of Technology Center for Computational Materials Science.

26 April 1995; accepted 29 August 1995

Imaging Pattern Formation in Surface Reactions from Ultrahigh Vacuum up to Atmospheric Pressures

H. H. Rotermund,* G. Haas, R. U. Franz, R. M. Tromp, G. Ertl

Two optical methods that allow pattern formation to be investigated at an arbitrary pressure are here applied to image concentration patterns of adsorbed species associated with heterogeneous catalytic reactions. In contrast to most surface physical techniques, these methods are not restricted to high vacuum conditions and thus bridge the "pressure gap." With carbon monoxide oxidation on a (110) surface of platinum as an example, the coupling mechanisms responsible for spatiotemporal self-organization in surface reactions were followed from reaction-diffusion control to the thermokinetic region, associated with phenomena not previously observed in pattern formation.

The applicability of most surface physical techniques is restricted to ambient gas pressures below about 10^{-3} mbar. This gives rise to a "pressure gap" between model studies conducted at low pressures and the conditions of "real" catalysis. Data measured at low pressures exploring the mechanism and kinetics of a heterogeneously catalyzed reaction can be theoretically extrapolated across a large pressure range (*1*); however, there are also cases in which the phenomena occurring on opposite sides of this gap are different in nature. This is the case for nonlinear effects causing spatiotemporal pattern formation on a reacting surface (*2*): At low pressures the conditions are nearly isothermal, and concentration patterns are formed by coupling of the reaction and surface diffusion. Phenomena of this type have been widely studied with the recently developed technique of photoemission electron microscopy (PEEM) (*3–5*). At higher pressures, on the other hand, finite temperature differences caused by variations of the heat release associated with the reaction give rise to thermokinetic waves governed by the heat conductance of the system, which to date have been imaged primarily by techniques based on infrared emission (*6*).

In this report we demonstrate how two optical methods may be used to image surface patterns at arbitrary pressure. With these techniques, the continuous range of coupling mechanisms responsible for spatiotemporal self-organization in surface reactions (for example, diffusion and heat conductance) becomes accessible to experimental investigation. The two techniques, ellipsomicroscopy for surface imaging (EMSI) and reflection anisotropy microscopy (RAM), are closely related and are based on changes of the degree of polarization of light reflected from a surface.

The EMSI technique is based on ellipsometry, which is well-established and has been used as an imaging method for characterizing structures on surfaces with thick-

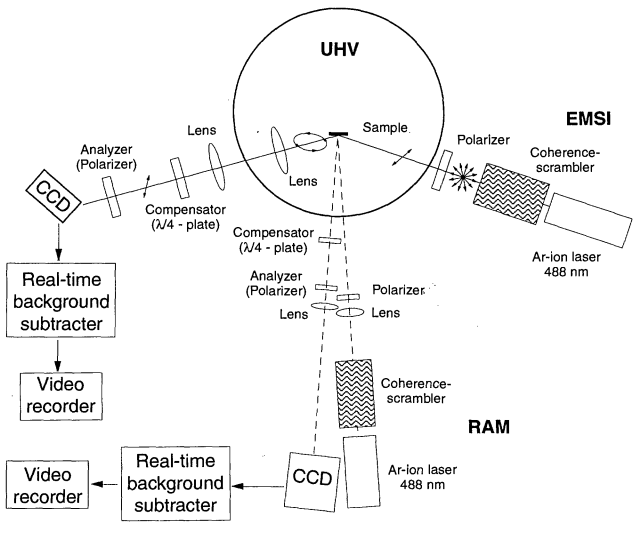

Fig. 1. Experimental setup for EMSI and RAM. Light from an Ar-ion laser (wavelength $\lambda = 488$ nm, power = 100 mW) is reduced in coherence as it passes through a vibrating multimode optical fiber; it is then linearly polarized and illuminates the surface at an angle of 70° with respect to its normal for EMSI (solid path) and close to normal incidence for RAM (dashed path). After reflection, the beam is imaged onto a charge-coupled device (CCD) chip by lenses (enabling magnifications between ×1 and ×50), after passing through a compensator ($\lambda/4$ plate) and being adjusted close to zero intensity by the analyzer. An image processor (Hamamatsu Argus 20) permits background subtraction in real time. Arrows indicate the polarization of the light for EMSI.

nesses greater than several nanometers (7). We developed the EMSI technique to allow real-time imaging of dynamic phenomena in distributions of submonolayer quantities of atoms adsorbed on a metal surface from ultrahigh vacuum (UHV) to atmospheric pressures. Although EMSI is presented here as a more qualitative tool, it should be possible to obtain quantitative information about the observed systems from measurements and corresponding calibration of the common ellipsometric parameters Δ and Ψ (8). Thus, in principle the concentrations of chemisorbed species on the surface could be inferred from the changes in Δ and Ψ relative to the clean surface; however, for practical purposes calibration of the brightness through well-defined adsorbed layers should usually be appropriate.

Sensitivity in surface imaging comparable to that with EMSI is achieved if the beam is reflected near normal incidence (Fig. 1). In this mode, the optical reflectivity along the two inequivalent directions of an anisotropic surface is probed; therefore, we denote this method as reflection anisotropy microscopy. It requires that the (azimuthal) polarization angle of the incident light be adjusted between the two principal axes of an anisotropic surface, such as the (110) plane of a face-centered-cubic crystal. This takes advantage of the fact that the anisotropy in reflectivity is often changed by the presence of a submonolayer coverage of adsorbates (9), caused by, for example, a surface reconstruction or the formation of an overlayer with a unit cell of different symmetry.

For both techniques, the reflected light is extinguished by appropriate settings of the compensator and analyzer, such that the image is dark for a uniform, featureless surface. For the EMSI image, local deviations of the ellipsometric parameters—that is, the complex refractive index and the thickness of surface layers—appear as brighter areas. For RAM, regions of different reflection anisotropy are contrasted. We conducted the experiments presented here in an UHV system using both methods independently, but EMSI and RAM can be applied simultaneously, thereby providing supplementary information.

We studied the catalytic oxidation of carbon monoxide on a Pt(110) surface, a system whose mechanism and dynamic properties have been explored in detail (4). The reaction proceeds through surface recombination of chemisorbed O and CO species (formed by adsorption of gaseous O_2 and CO), whereby the CO_2 produced by the reaction is immediately released into the gas phase. Under certain conditions of temperature T and partial pressures p_{O_2} and p_{CO}, the reaction rate becomes oscillatory or even chaotic, and the surface concentrations of adsorbed O and CO are not uniform, but rather exhibit spatiotemporal patterns between regions of high O coverage (with a high reactivity) and regions of high CO coverage (less reactive). These patterns have been studied in detail at partial pressures below 10^{-3} mbar with the PEEM technique (10).

In experiments at pressures below 10^{-3} mbar, where PEEM is applicable, EMSI and RAM revealed the same patterns observed with PEEM, but with a much-enlarged field of view, up to the full sample size. This allowed the observation of patterns on a larger length scale. Contrast was observed in RAM images (Fig. 2) as a result of differences in the anisotropy of surface reflectivity. This was verified by turning the azimuth of the sample during pattern formation. When the [001] or [1$\bar{1}$0] directions of the crystal were aligned with the plane of polarization of the incident light, contrast was lost. Dark and bright areas in the image can be attributed to domains predominantly covered by CO and O, respectively. This was verified by comparison with experiments in which the surface was uniformly covered either by CO or O.

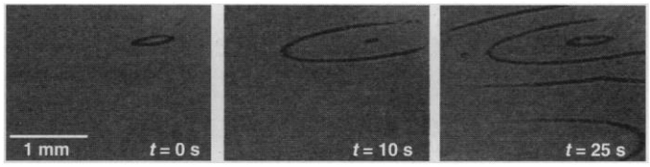

Fig. 2. Pattern formation during the CO oxidation on Pt(110) for $p_{O_2} = 4 \times 10^{-4}$ mbar and $p_{CO} = 6.2 \times 10^{-5}$ mbar at $T = 494$ K, recorded with RAM, showing the development of a CO-rich target pattern surrounded by O-rich areas of the surface. Target patterns observed previously (under different conditions) with PEEM (10) exhibited wavelengths on the order of 10 μm; the wavelength here is about 1 mm.

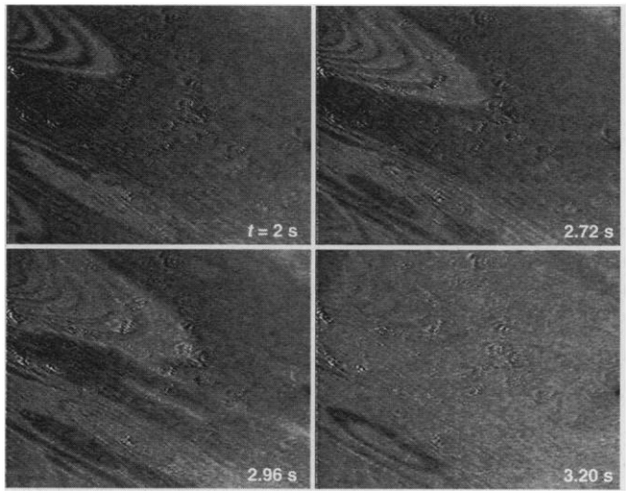

Fig. 3. Transition from the less reactive (CO-rich) into the highly reactive (O-rich) state, recorded by EMSI. At $t = 0$, p_{CO} was lowered from 0.07 to 0.06 mbar with $p_{O_2} = 0.5$ mbar and $T = 550$ K. At $t = 2$ s, an O-rich spiral wave appears and then propagates into the CO-covered region. Extinction was adjusted for the homogeneously CO-covered surface. Areas covered by O thus appear brighter. The image diameter is 1.4 mm.

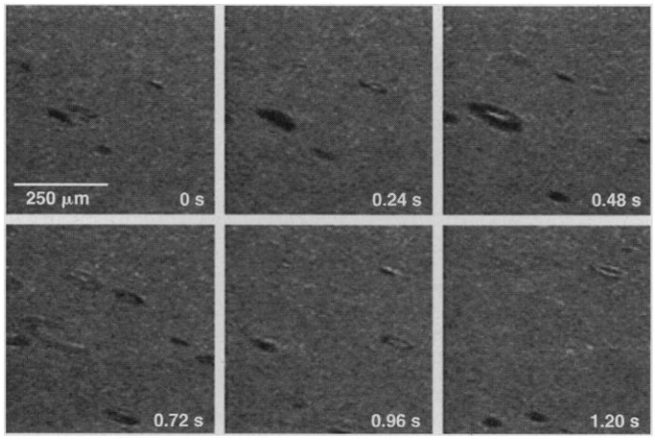

Fig. 4. Raindrop-like patterns at $p_{O_2} = 2.22 \times 10^{-2}$ mbar, $p_{CO} = 5 \times 10^{-3}$ mbar, and $T = 534$ K observed with EMSI.

H. H. Rotermund, G. Haas, R. U. Franz, G. Ertl, Fritz-Haber-Institut der Max-Planck-Gesellschaft, Faradayweg 4-6, D-14195 Berlin, Germany.
R. M. Tromp, IBM Research Division, Yorktown Heights, NY 10598, USA.
*To whom correspondence should be addressed.

Under low-pressure conditions ($<10^{-3}$ mbar), the sample temperature remained constant, unaffected by variations of the surface composition and reactivity. Such patterns have previously been modeled theoretically by appropriate reaction-diffusion equations (*4*, *5*). However, when the pressure was increased by more than two orders of magnitude (into the pressure range not accessible by PEEM), the situation changed markedly. Because of the higher turnover rate, the sample temperature was considerably affected by the released heat of reaction. For the gas composition with the highest turnover, the increase in temperature was as high as 40 K at a total pressure of 0.5 mbar. When the CO/O_2 partial pressure ratio was further increased, the surface changed from the reactive into the less reactive state, associated with a rapid decrease of the sample temperature. To reestablish a high reaction rate, we had to intermediately lower p_{CO}. The resulting transient state is reflected in EMSI images (Fig. 3). At t = 2 s, an O-rich spiral wave appeared. This spiral propagated into the CO-covered region, such that after 3 s, roughly half of the imaged surface area was in the reactive O-rich state. Because of the increase of reactivity, the sample temperature rose, which further enhanced the decrease of the CO concentration by desorption, such that after about 3.2 s, the whole surface was in the predominantly O-covered and highly reactive state—that is, had turned bright. The speed of the reaction front was determined from the video frames between the last two images of Fig. 3 to be about 5 mm/s.

We have been able to observe pattern formation and propagating reaction fronts up to total pressures of 1 atm. Limitations at even higher pressures were encountered because the UHV chamber used in the experiments is unsuitable for such conditions.

A previously unseen type of pattern was found (Fig. 4) at $p_{O_2} = 2.22 \times 10^{-2}$ mbar. Its features are reminiscent of target patterns known from pure reaction-diffusion behavior at lower pressures (*4*). However, while the latter are periodically emitted from fixed trigger centers (presumably surface defects) and propagate continuously, the present patterns appear at random, like raindrops on a flat water surface rapidly dying out after a short propagation length. This behavior may be described by the superposition of reaction-diffusion and thermokinetic effects. The pronounced damping of wave propagation and the role of nonisothermal effects in this system will have to be analyzed in the future by detailed theoretical modeling.

The rather simple optical methods EMSI and RAM presented here allowed the investigation of pattern formation associated with heterogeneously catalyzed reactions from UHV up to atmospheric pressures. An upper pressure limit for the applicability of these methods is not apparent. In addition, with the spatial resolution principally limited by diffraction, these methods will enable the study of other surface processes occurring at length scales from the submicrometer up to several millimeters, and the present temporal resolution of 20 ms can certainly be improved significantly.

REFERENCES AND NOTES

1. P. Stoltze and J. K. Nørskov, *Phys. Rev. Lett.* **55**, 2502 (1985).
2. M. Eiswirth and G. Ertl, in *Chemical Waves and Patterns*, K. Showalter and R. Kapral, Eds. (Kluwer, Amsterdam, 1995), p. 447.
3. H. H. Rotermund, W. Engel, M. Kordesch, G. Ertl, *Nature* **343**, 355 (1990).
4. G. Ertl, *Science* **254**, 1750 (1991).
5. M. Bär, S. Nettesheim, H. H. Rotermund, M. Eiswirth, G. Ertl, *Phys. Rev. Lett.* **74**, 1246 (1995).
6. V. V. Barelko, I. I. Kurachka, A. G. Merzhanav, K. G. Shkadinskii, *Chem. Eng. Sci.* **33**, 805 (1978); S. L. Lane and D. Luss, *Phys. Rev. Lett.* **70**, 830 (1993); F. Quin, E. E. Wolf, A. C. Chang, *ibid.* **72**, 1459 (1994).
7. R. Reiter, H. Motschmann, H. Orendi, A. Nemetz, W. Knoll, *Langmuir* **8**, 1784(1992); R. F. Cohn, J. W. Wagner, J. Kruger, *Appl. Opt.* **27**, 4664 (1988).
8. J. J. Carroll, T. E. Madey, A. J. Melmed, D. R. Sandstrom, *Surf. Sci.* **96**, 508 (1980).
9. D. A. Woolf *et al.*, *Phys. Rev. B* **51**, 4691 (1995).
10. S. Jakubith, H. H. Rotermund, W. Engel, A. von Oertzen, G. Ertl, *Phys. Rev. Lett.* **65**, 3013 (1990).

11. We acknowledge B. E. Argyle and W. Schrittenlacher for numerous useful suggestions and illuminating discussions.

4 August 1995; accepted 20 September 1995

Nanoscale Complexity of Phospholipid Monolayers Investigated by Near-Field Scanning Optical Microscopy

Jeeseong Hwang,* Lukas K. Tamm, Christine Böhm, Tirunelveli S. Ramalingam, Eric Betzig,† Michael Edidin

Near-field scanning optical microscopy of phospholipid monolayers doped with fluorescent lipid analogs reveals previously undescribed features in various phases, including a concentration gradient at the liquid-expanded/liquid-condensed domain boundary and weblike structures in the solid-condensed phase. Presumably, the web structures are grain boundaries between crystalline solid lipid. These structures are strongly modulated by the addition of low concentrations of cholesterol and ganglioside G_{M1} in the monolayer.

Lipid monolayers have been used to study two-dimensional systems, to construct organized arrays and matrices, and to model biological membranes (*1*). An understanding of their structure is critical to all of these efforts. At the molecular level, much has been learned from x-ray and electron diffraction (*2*), scanning tunneling microscopy (STM), and atomic force microscopy (AFM) (*3*). It is also possible to analyze lipid monolayers on a larger scale by far-field epifluorescence microscopy (FFM) (*4*–*7*) of monolayers doped with fluorescent lipid analogs. Such studies have shown that, in the fluid-solid coexistence region, lipid monolayers exhibit domain structures. The size and shape of these domains vary with temperature, pressure, and the chemical composition of the monolayer. In particular, low concentrations of certain compounds (such as cholesterol) alter the line tension at the boundary between two coexisting phases, thereby changing the domain

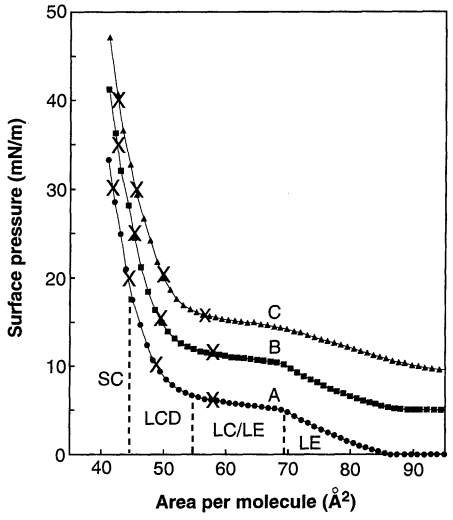

Fig. 1. The πA isotherms of (curve A) DPPC/0.5 mol % Bodipy-PC, (curve B) DPPC/0.5 mol % Bodipy-PC/1 mol % cholesterol, and (curve C) DPPC/0.5 mol % Bodipy-PC/0.5 mol % ganglioside G_{M1} monolayers at the air-water interface. For clarity, isotherms B and C are shifted upward with an offset of +5 and +10 mN/m, respectively, in surface pressure. Four different regions (LE, LE/LC, LCD, and SC) corresponding to different lipid phases are distinguished. Points at which the monolayers were sampled are marked by X's on the curves.